RSC Advances

ROYAL SOCIETY OF CHEMISTRY

www.rsc.org/advances

Journal Name

RSCPublishing

ARTICLE

Luminescent, Ferromagnetic Silver Glyconanoparticles: Synthesis to Annealing-induced Substrate Specific Transformation

Cite this: DOI: 10.1039/x0xx00000x

Received ooth January 2012,
Accepted ooth January 2012

DOI: 10.1039/x0xx00000x

www.rsc.org/

Jaba Mitra[a, b] *and Ashutosh Sharma**[a],

A one-pot, economically viable 'green' synthesis of silver glyconanoparticles is reported with sugarcane juice. The morphology and size of particles could be tuned by changing reaction conditions like the temperature, pH, concentration etc. Sugar and non-sugar biomolecules in sugarcane acted as reducing and/or capping agents in the synthesis. These glyconanoparticles exhibited exceptional photoluminescence and ferromagnetism at room temperature. This general route can be employed for the synthesis of other noble metal nanoparticles. Annealing of silver nanoparticles on underlying polymer fibers yielded unprecedented hollow helical structures as opposed to rods obtained on silicon wafer. A surface-assisted self-assembly mechanism has been proposed to explain the peculiar morphology of annealed structures. Photoluminescence of the as-annealed structures has also been demonstrated. These hollow and solid rods have potential applications in the fabrication of nano-circuits and optoelectronics.

Introduction

Nanoparticles with high surface to volume ratio, broken translational symmetry and reduced co-ordination of surface atoms display significantly different properties compared to bulk materials. Electrical, magnetic, optical as well as catalytic properties of nanomaterials can be tuned according to their size, shape and composition.[1] Silver nanocrystals have attracted immense attention due to their applications related to surface plasmon resonance (SPR), surface enhanced Raman scattering (SERS), optical labeling and biological sensing.[2-5] Magnetic silver nanoparticles would open new opportunities in magnetic resonance imaging (MRI), hyperthermic treatment for malignant cells, site-specific drug delivery and also in manipulating cell membranes.[6, 7] Syntheses of Ag nanoparticles have been achieved by employing varied techniques, some of which involve expensive, hazardous and non-eco-friendly materials. [8-11]

There has been a great impetus in self-assembly driven hybrid nanomaterials from inorganic nanoparticles and biomolecules.[6] Nanoparticles and biomolecules being of similar length scales, their combination can provide interesting tools to probe the mechanism of various biological processes and also as chemical means to manipulate biological components.[12, 13] Such composites with gold nanoparticles functionalized with protein and DNA are being developed for cellular interaction studies.[14, 15] Comparatively, silver nanoparticles are much less explored.

Glyconanoparticles i.e. nanoparticles having an outer coating of carbohydrates have gained recent attention. Zhang *et al.*[16] used a three step ligand exchange process to prepare hybrid silver glyconanoparticles. But the carbohydrates were not covalently attached to the nanoparticles. Yang *et al.*[17] demonstrated that electrostatic interaction between the carbohydrate and nanoparticle enhance nanoparticle stability. Nazir *et al.*[18] showed remarkable anti-tumor potency of silver glyconanoparticles synthesized using table sugar as reducing agent. That apart, several well-known commercial products like tea,[19, 20] coffee[20] etc. have been leveraged in silver chemistry.

In this study, we have used sugar cane juice, a common beverage in India for bio-reduction of silver salts to produce silver nanoparticles. Sugar cane (*Saccharum officinarium*) constituted primarily by glucose, fructose and sucrose, can serve both as a reducing agent and stabilizing agent, as the sugar molecules can form complexes with the silver particles to arrest their unwanted aggregation. The effect of reaction conditions have been studied by varying the temperature, pH, reaction time and precursor concentration. We show that the crystalline silver nanoparticles, thus synthesized have exceptional photoluminescence and magnetic properties that can be tuned by particle size. We focus on the observed soft-ferromagnetic property of these glyconanoparticles which has

found almost no mention in the vast literature pertaining to silver nanoparticles. Additionally, these spherical nanoparticles can be converted to vertical rod-like or helical structures, depending on the underlying substrate, on annealing at 800 ^{o}C. Such structures were also found to retain the luminescent properties of the parent nanoparticles. Annealing of silver glyco-nanoparticles into complex shapes can be harnessed into ordered bio-molecular devices, superfine nanocircuits and other nanoscale machineries.[21]

Materials and Methods

Reagents Used

Sugar cane juice freshly procured from the market was filtered and diluted with de-ionized water. Silver nitrate, sucrose, glucose, PAN (poly-(acrylonitrile), M_w 1,50,000) and DMF (N,N-Dimethylformamide) were procured from Sigma Aldrich.

Synthesis

In a typical experiment, a definite concentration (0.05, 0.1, 0.2 or 0.4 M) of silver nitrate solution was reacted with sugar cane juice or sucrose (13%) and glucose (2%) solution at predetermined temperatures (60 ^{o}C, 100 ^{o}C and 150 ^{o}C). After reaction, the suspension was collected, washed and dispersed in deionized water for further characterizations. As the degradation of fructose is anticipated under the reaction conditions (temp ≥ 60 ^{o}C), a mixture of sucrose (13%) and glucose (2%) was used to emulate the "sugar" composition of cane sugar.

PAN fibers were electrospun from a solution of 8 wt% PAN in DMF at a constant flow rate of 2 µL/min and applied voltage of 1.2 kV/cm. The silver nanoparticles were adsorbed onto electrospun PAN-fibers overnight. The nanoparticle-fiber ensemble was annealed at 250 ^{o}C for 1 h, for stabilization of PAN fibers, prior to annealing at 800 ^{o}C. The results were compared with those obtained with silver nanoparticles deposited on silicon wafers under identical conditions.

Characterization

Synthesized silver glyconanoparticles (as-synthesized and annealed) were studied by Field Emission Scanning Electron Microscopy and Energy dispersive X-ray Spectroscopy (EDX) (FESEM, Quanta 200, FEL Germany, SUPRA, Zeiss, Germany). The accelerating voltage was maintained at 10 kV. The samples for FESEM/EDX were prepared by depositing a suspension of silver nanoparticles in de-ionized water on clean silicon wafers and dried under ambient conditions. TEM analysis was done with EI Technai 20 U Twin Transmission Electron Microscope operated at 200 kV. Carbon coated copper grid (mesh size 400) procured from Electron Microscopy Sciences, Hatfield, PA was used to prepare the TEM samples.

FTIR (Bruker Vertex-70) analysis of glycomolecules adsorbed onto the silver nanoparticles was recorded as pressed KBr pellets over a range of 400-4000 cm^{-1}. Confocal Micro-Raman microscope (CRM 200, WITec, Germany with λ = 543 nm) was also used to characterize the particles. Raman spectra was recorded at least three different positions for each sample. The crystallinity of the samples, in the form of thin films was determined by X-ray diffraction (PANalytical X'pert PRO MRD) at wide angle.

UV-Visible spectra of silver nanoparticles dispersed in de-ionized water were recorded on a Cary Varian 50 UV/VIS spectrophotometer. The photoluminescence (PL) emission was recorded in PerkinElmer *LS*55 fluorescence spectrometer by using quartz cells of 10 mm path length. Magnetic hysteresis curves were obtained from Magnetic Charger (Princeton Equipments). The dried samples in Teflon tapes were placed parallel to the magnetic field which was varied between ± 15000 Oe.

Results and Discussions

The primary constituents of sugarcane juice are sucrose, glucose and fructose. Thermally catalyzed sucrose hydrolysis yields glucose and fructose under acidic conditions.[22] As the reactions are mostly carried under slightly acidic conditions (pH of sugarcane juice is 5.5), at temperatures above 60 ^{o}C, sucrose disintegrates into glucose and fructose, of which the latter degrades (>60 ^{o}C) leaving glucose to reduce silver nitrate (Scheme 1, ESI).

Reduction of silver nitrate was manifested by the gradual evolution of color of the solution from dark yellowish to brown and finally black. The sugar cane juice reduces silver nitrate to silver nanoparticles and also acts as a capping agent to forestall aggregation. The UV-Vis spectra of the synthesized particles are characterized by an intense peak at around 410 nm, corresponding to the surface plasmon resonance and out of plane resonance of silver nanoparticles (Figure 1). A gradual red shift to ~ 440 nm was observed with time, due to coalescence and growth of the particles.

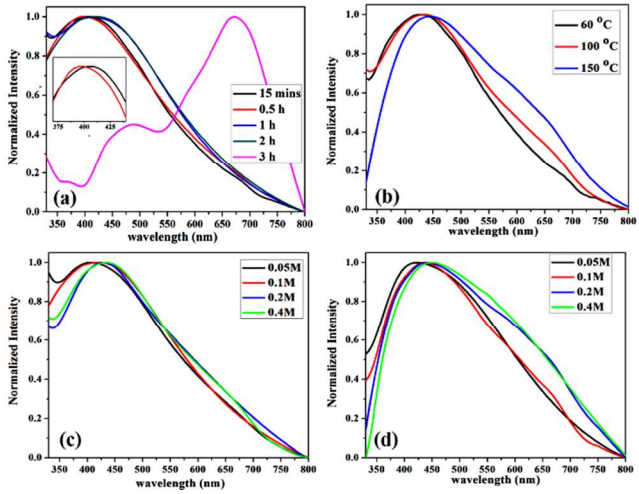

Figure. 1. UV-Vis spectra of Ag glyconanoparticles reduced with sugar cane juice (a) increasing reaction times at 100 ^{o}C, at 0.1 M salt concentration (expanded view in the inset shows blue shift in the absorption maxima from 15 mins to 30 mins), (b) temperature after 2 h reaction at 0.4 M salt concentration, (c, d) concentration after 2 h, at (c) 100 ^{o}C and (d) pH = 8.

At the onset of reaction, the rate of reduction of silver salt is substantially higher than the adsorption of capping sugar molecules on the nanoparticle surface. Hence, the smaller nanoparticles generated, aggregate into larger nanoparticles. The larger nanoparticles being unstable, disintegrates into their smaller counterparts,[23] as manifested by a slight blue shift in UV-Vis spectra from ~407 nm to ~400 nm after 30 mins (Figure. 1a). As the reaction progresses, more and more silver ions are reduced and the particle size ceases to decrease. This in turn accounts for a broadening of the absorption maxima with time. After 3 h, additional weak absorbance at ~360 and strong absorbance at 670 nm was observed (Figure. 1a). These peaks have been identified as the out-of plane quadrupole resonance and in-plane dipole plasmon resonance of triangular nanoprisms respectively.[9] Scanning electron micrographs support the presence of such prisms (Figure. S3a, ESI). At higher silver salt concentrations, a red shift in absorption maxima is observed, which is consistent with the increase in the size of the silver cluster (by condensation followed by coalescence) due to the availability of less amount of capping biomolecules.

In addition to reducing sugars, sugar cane juice contains amino-acids and antioxidants like flavonoids and polyphenols. Presence of these organic non-sugar molecules affect the particle size and shape distributions, in view of their modified capping capability compared to sugar solution. This was validated by our observation of reduced particle size and uniformity of shapes obtained using sugarcane juice compared to the particles synthesized using sugar solution as reducing agent under identical experimental conditions (Figure. S1, ESI). The characteristic broad IR signal of sugar molecules shifts from 3260 cm-1 to 3330 cm^{-1} (Figure S2, ESI). Another high frequency shift in C=O stretching from ~1750 cm-1 to 1635 cm-1 points to the coordination of sugar moieties with Ag nanoparticles.[24] Probable contributions from non-sugar residues on the silver nanoparticles, e.g., amide I and II stretching bands at 1635 and 1540 cm^{-1} and C=O stretching of flavonoids can be identified (Figure S2b, ESI). Raman imaging also corroborates occurrence of different phases in the silver nanoparticles (Figure. S3, ESI).

SEM, TEM and EDX Analysis

SEM analysis reveals a decrease in particle size from ~8 nm to ~5 nm (Figure 2a, b) supporting the slight blue shift observed in UV-Vis spectra. Further increase in the reaction time results in aggregated particles of diameters ~10 and 13 nm (after 1 and 2 h respectively), prior to the formation of nanoprisms of edge length ~100 nm and thickness ~ 30 nm (Figure. S4a, ESI). Spherical particles with increasing diameter are formed with increasing salt concentrations (~9, 13, 18 and 23 nm at salt concentrations of 0.05, 0.1, 0.2 and 0.4 M respectively) (Figure. 3). A similar trend was observed with increasing temperature (diameter ~ 12 and 33 nm at 60 and 150 ^{o}C respectively) after 2 h reaction (Figure. S5, ESI).

In addition to the peaks for Ag in the EDX spectra of Ag glyconanoparticles, prominent presence of carbon, nitrogen and oxygen are observed (Figure S6, ESI) which can be accounted for, considering the presence of organic sugars and non-sugars as capping moieties.

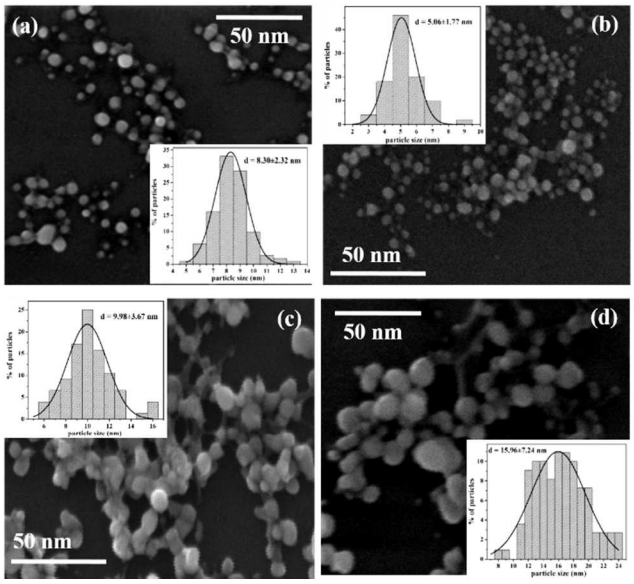

Figure. 2. FESEM images of silver glyconanoparticles synthesized at 100 ^{o}C with sugar cane juice and 0.1 M silver salt concentration as a function of reaction times: (a) 15 mins, (b) 30 mins, (c) 1 hr and (d) 2 h. Inset shows the respective particle size distributions.

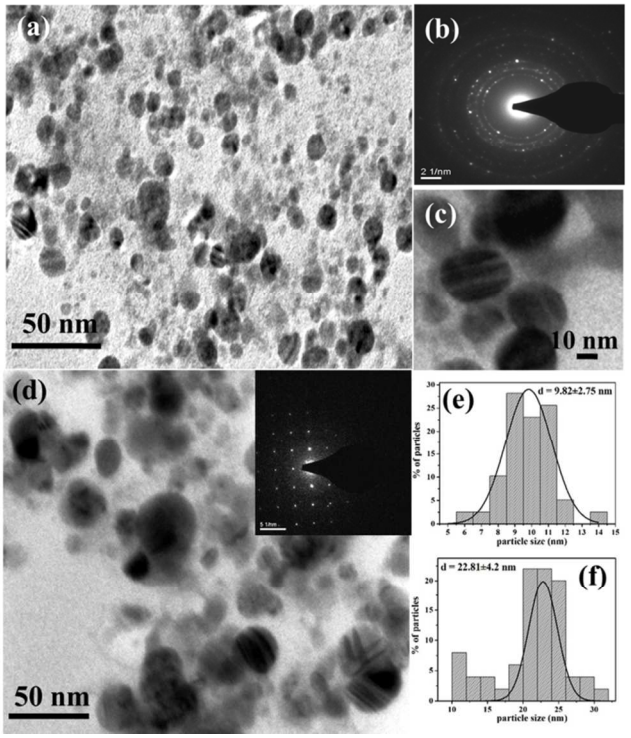

Figure. 3. TEM images of silver glyconanoparticles synthesized at 100 ^{o}C for 2 h at silver salt concentration of (a) 0.1 M and (d) 0.4 M with sugar cane juice. (b) and (d) inset shows the SAED patterns of (a) and (d) respectively. (c) Magnified view of (a) showing staple faults. (e, f) Particle size distributions of (a) and (d) respectively.

Formation of nano-triangles can also be observed at 150 °C (Figure. S5, ESI). The selected area electron diffraction (SAED) (Figure. 3) pattern corresponds to face-centered cubic (FCC) Ag nanoparticles. Enhancement in crystallinity can be observed with increase in particle size. A similar finding has also been reflected in the XRD analysis (see later).

In contrast, Ag nanoparticles generated with sugar solution (glucose and sucrose only), resulted in a wide variety of shapes (Figure S4b, ESI), suggesting an influence of organic non-sugar constituents of sugar cane juice towards controlling the particle shape.

XRD Analysis

Characteristic Bragg diffraction peaks for crystalline Ag glyconanoparticles are observed from XRD analysis having 2θ values of 38.2, 44.3, 64.5, 77.4 and 81.7° corresponding to [111], [200], [220], [311] and [222] planes of FCC lattice (Figure. 4).[33] Ag crystals preferentially grow along the [111] facet with increase in concentration, reaction time and temperature. Newer lattice planes ([200], [220], [311] and [222]) are generated over time and with increasing salt concentration as more and more silver ions are reduced. Over-representation of the [111] plane is a probable consequence of the evolution of spherical particles into triangular plates or nanoprisms.[26] A similar growth along [111] plane was observed for silver nanoparticles synthesized with sugar solution (Figure. S7, ESI). High crystallinity manifested in the XRD patterns can be explained in accordance to 'oriented attachment' (OA) mechanism.[27]

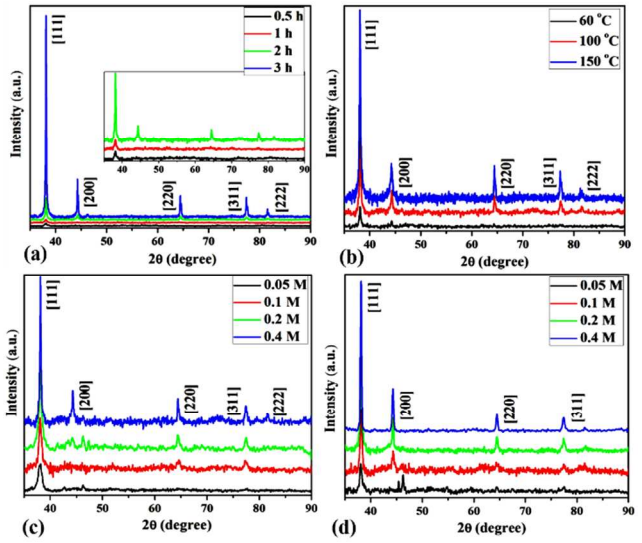

Figure. 4. XRD patterns of Ag nanoparticles as functions of (a) reaction times at 100 °C, at 0.4 M salt concentration temperature after 2 h reaction (inset shows an expanded view up till 2h of reaction), (b) temperature at 0.4 M salt concentration after 2h reaction, (c, d) concentration, after 2 h at 100 °C (c) and pH ~ 8.0.

Initially, the reduction of silver salt proceeds rapidly, generating spherical and pseudospherical particles.[28] As the reaction progresses, the rate of Ag^+ reduction decreases, indicating presence of twin planes in the nanoparticles.[29] The re-entrant grooves created by twin planes and stacking faults cause preferential attachment of adatoms with lower nucleation energy to form a fresh atomic layer. Thus growth is enhanced parallel to the twin planes, extending the lowest energy crystal facet and forming triangular nanoprisms. Stacking faults, are created during the direct coalescence of particles via OA. Prolonged reaction time results in the shape conversion of these nanotriangles into spheroids according to the Gibbs-Thompson effect, which proposes the decrease in stability of sharp corners of the nanotriangles due to higher curvature and surface energy. Thus dissolution of Ag atoms from the less stable corner sites and re-adsorption on to the more stable sites with low curvature and surface energy occur overnight.[30] Incidentally, growth occurs faster in absence of organic non-sugars (Figure. S7, ESI). In view of the differences in shape distributions of silver nanoparticles synthesized under sugar and sugar cane reduction, it might be surmised that non-sugar moieties stabilize the intermediate particle conformations, i.e. modify the duration of the steps, provided there is no effective change of the growth mechanism.

Photoluminescence Study

Direct metal-metal interactions result in different HOMO-LUMO gaps and contribute to fluorescence bands in ligated d^{10} metals. On excitation at 330 nm, strong emission bands at 370 and 400 nm and a weak shoulder at 495 nm were observed. These could be assigned to the fluorescence emissions from E_3 to E_0 for 370 nm, E_2 to E_0 for 400 nm and E_1 to E_0 for 497 nm.[31] The strong band ~410 nm could be the SPR band of Ag glyconanoparticles (Figure. 5a) and can be attributed to the absorption-scattering mechanism. A slight blue shift of this band with respect to the original scattering peak can be explained by the abundance of available electrons near the initial energy of laser excitation.[32] The relative predominance of this band in Ag glyconanoparticles compared to that in sugar-reduced Ag nanoparticles can be explained by the larger size of glyconanoparticles obtained in the former, under identical reaction conditions. As the size of the particle increases, the ratio of surface atoms and Ag-Ag interactions decrease, and hence the absorption-scattering phenomena predominate. The broadband at ~ 460 nm can be assigned to the interaction of the interface electrons with the capping ligands (Figure. 5b, c).[33] On excitation at the characteristic SPR of silver nanoparticles, two intense spatially separated peaks at around 540 and 560 nm were observed (Figure. 5c). Recently, amine ligated silver clusters were reported to have an emission maximum centered at 590 nm.[34] Two bands could be due to the presence of sugar and non-sugar capping agents on the Ag surface. Only the 540 nm band could be observed in sugar-reduced particles.

Multiple peaks in the excitation spectra are suggestive of the presence of multiple emission centers in the silver nanoparticles (Figure. 5d-f). The excitation maxima obtained at around 240 - 290 nm have been previously attributed to the absorption by silver clusters of different atomic sizes.[35] Very weak bands

corresponding to absorption from different sizes of silver clusters could also be observed.[35] The difference in excitation spectra for emission at 540 (Figure. 5e) and 560 nm (Figure. 5f), advocate presence of chemically different emissive species, which is plausible due to the presence of both sugar and non-sugar capping moieties in cane sugar.

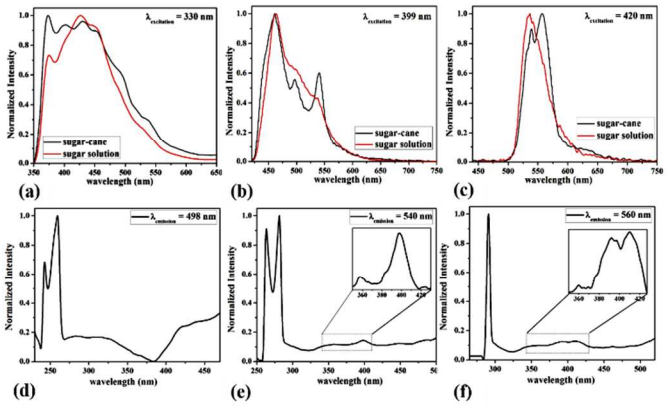

Figure. 5. Representative PL (a-c) emission spectra of Ag nanoparticles at excitation wavelengths of (a) 330, (b) 399 and (c) 420 nm and (d-e) excitation spectra at emission wavelengths of (d) 498, (e) 540 and (f) 560 nm. Inset in (e, f) delineates presence of minor peaks.

Magnetism

As particle dimensions approach that of magnetic domains, interactions with capping agents, chemical environment, defects, vacancies, inclusions and imperfections present in the material surface synergistically induce magnetism in otherwise diamagnetic systems.[36] Bulk Ag ($4d^{10}$ system) is diamagnetic with a susceptibility of $\chi = -1.8*10^{-7}$ emu/g Oe. [37] Magnetic properties of Ag glyconanoparticles vary with the synthesis conditions (i.e, temperature, salt concentration, reaction time or reducing agent, Figure 6). The magnetic hysteresis loops demonstrate coercive field values ~100 Oe at room temperature, signifying soft magnetism. Interestingly, the coercive field reported here is somewhat higher than that reported for thiol-capped Ag nanoparticles.[37] The saturation magnetization and coercive field values decreased with increasing particle size.

The magnetic moment in a nanoparticle arises from a surface macro-moment and its core counterpart. Mulliken population analysis asserts a charge transfer from outer to the core silver atoms, thereby inducing an excess charge of 0.8 electrons on the latter. The large co-ordination number of the central silver atom effects substantial overlaps of its 4d orbitals with those of the outer silver atoms, resulting in the depopulation of the latter's states.[38] As the magnetization of the core opposes that of the surface, there is a significant reduction in saturation magnetization with increasing particle diameter as shown in Figure. 6d. A decrease in coercive field values is also observed with increasing particle size (Figure. S8b, ESI).

It has been proposed that there is an imbalance between electrons with up and down spins near the surface when the nanoparticle diameter is below the critical diameter D_o (~ 3nm for Ag). [39] Spin polarization vanishes above the critical diameter rendering the particle effectively diamagnetic. However, we recorded room temperature saturation magnetization values between 0.097 and 0.01 emu/g of Ag corresponding to average particle diameters ranging from ~9 to 33 nm, which are much higher than the critical diameter of Ag. PL studies have suggested the presence of silver clusters on the glyconanoparticles. Thus we propose that the spin-correlation region is limited only within the shell of magnetic clusters, within a depth given by the critical radius and the core has negligible contribution towards ferromagnetism.[39] It is known that coalescence of nanocrystals is energetically more favorable when magnetic moments are aligned;[36] hence, some residual magnetism is probably retained even at higher particle dimensions.

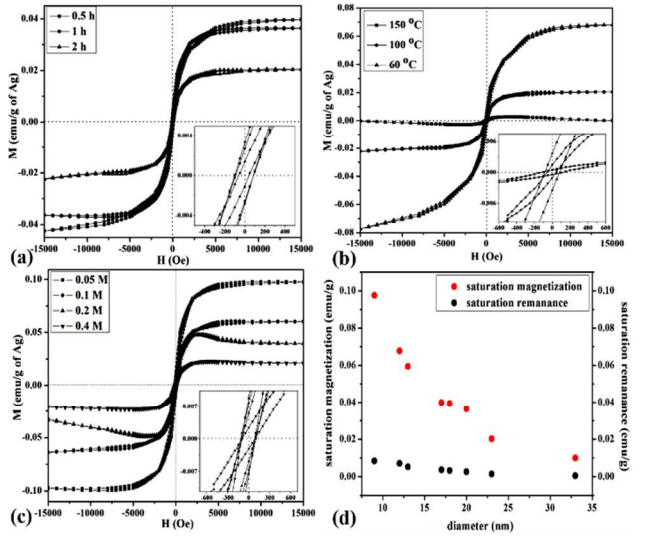

Figure. 6. Magnetic hysteresis loops of Ag nanoparticles as functions of (a) reaction times at 100 °C, at 0.4 M salt concentration (b) temperature after 2 h reaction at 0.4 M salt concentration, (c) concentration at 100 °C, after 2 h and (d) nanoparticle size-dependence of saturation magnetization and remanance.

Annealing of as-synthesized silver glyconanoparticles

The Ag glyconanoparticles (synthesized after 2 h reaction at 100 °C at 0.4 M salt concentration in sugar-cane juice) were adsorbed onto electrospun PAN fibers overnight. FESEM images revealed somewhat inhomogeneous distribution of the silver nanoparticles on the fiber surfaces (Figure. 7a). Annealing of the glyconanoparticles as is (i.e. on silicon wafer) and on PAN fiber at 250 °C (ensuring the cross-linking of electrospun PAN fibers) for 1 h resulted in silver nano-spheroids (Figure. 7b, e). It can be assumed that with the decomposition of the capping ligands (predominantly the sugar molecules which decomposes over 170 °C[40]) at 250 °C, silver nanoparticles coalesce into bigger structures: ~ 238 nm and ~ 152 nm on silicon wafer and PAN surface respectively (Figure. S9, ESI). These nano-spheroids are indicative of presence of multiple facets. Courty *et al.*[41] had demonstrated coalescence and recrystallization of silver nanoparticles into nanotriangles on mild annealing, on amorphous carbon and HOPG substrates.

It can be argued that the differences in morphologies are induced by the substrates. The cross-linked PAN fibers cater for self-organization of silver nanocrystals over a short distance, whereas on the crystalline silicon wafer surface, a comparatively long range order prevails and larger and more-faceted particles are formed. Ease of diffusion on silicon wafers causes faster recrystallization resulting in a wide size-distribution of more-faceted spheroidal particles.

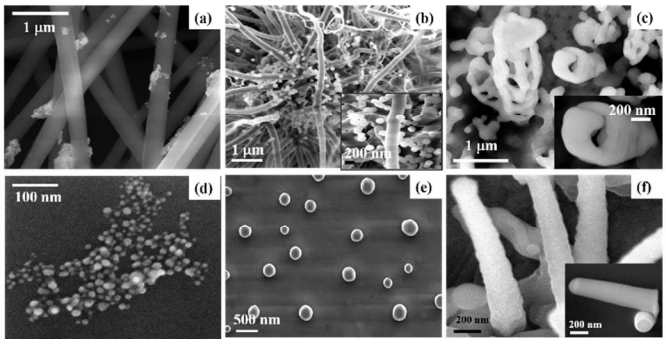

Figure. 7. (a) Silver nanoparticles adsorbed on PAN fibers. (b, c) Annealing of (a) at 250 and 800 °C. (d) Silver nanoparticles on silicon substrate. (e, f) Annealing of (d) at 250 and 800 °C.

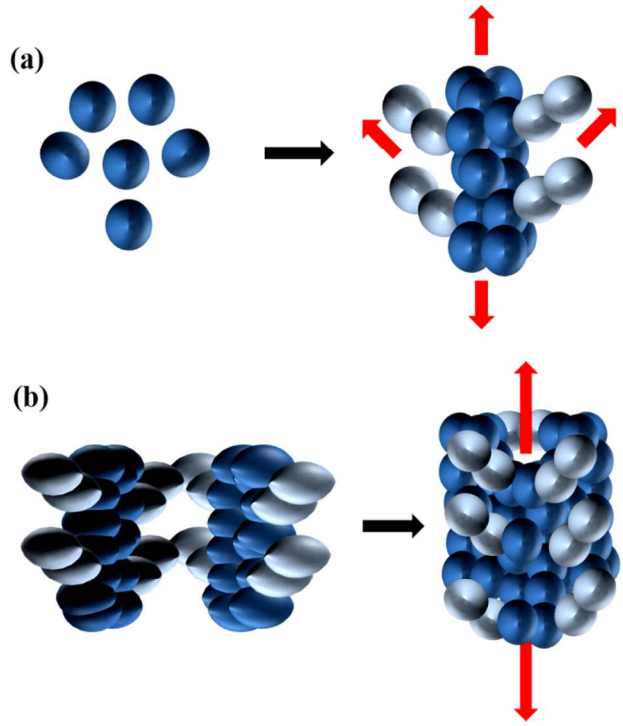

Figure. 8. Mechanism showing (a) self-assembly of silver nanoparticles into dendrimeric structures and (b) their subsequent assembly into helical structures. Color differentiates the central column from the branches.

The glyconanoparticles were further annealed at 800 °C (Figure. 7c, f). The FESEM images showed the presence of rod-like and hollow helical structures in the respective cases. A rough mechanism has been shown in Figure. 8. At higher annealing temperature (800 °C), underlying PAN-fibers are depleted and the large silver nanoparticles generated previously, self-assemble into dendrimeric structures, with several columns of silver nanoparticles in the center (Figure. 8a, S10, ESI). With the progress of reaction, multiple such structures join together and further deposition of Ag occurs in the spaces between the side branches to form helical structures (Figure. 8b). In few instances, with the progress of reaction, there is further deposition of silver nanoparticles in the spaces between the side branches and concomitant formation of hollow rod-like structures. At the onset, these structures grow vertically as Ag nanoparticles prefer deposition on themselves compared to the surface. With more and more deposition of silver, they gradually tilt towards the surface. Such growth has also been observed by Radha *et al*.[42] with giant gold nanoplates. In stark contrast, absence of underlying PAN fibers resulted in solid structures. Assuming, similar growth mechanism for both cases, it can be assumed that the PAN fibers help in preserving the hollowness as the Ag particles are only deposited around them and the hollowness remains after the PAN layer is removed at high temperature. As annealing is carried out at a temperature much higher than the Tamman temperature (643 K), mobility of the silver surface atoms leads to restructuring of the lattice.[43] EDX mapping of the helical structures depicted an abundance of oxygen on the surface (Figure. S11, ESI). As, at temperatures around 800 °C silver oxide decomposes, excess of oxygen can be attributed to its extensive adsorption on silver during annealing.

Green and red emission (cut-off filters 488nm and 561 nm) could be detected from the helical structures as evident from their fluorescence micrographs (Figure. S12, ESI). The intrinsic photoluminescence form the silver nanoparticle building blocks as well as the presence of adsorbed oxygen might synergistically affect the fluorescent properties of the synthesized helical structures.

Three intense peaks centered at 450, 650 and 950 cm^{-1} are evident from the Raman spectra of the annealed helices (Figure. S13, ESI). Annealing at a high temperature induces dissolution of oxygen in the silver. The peak at 450 cm^{-1} can be assigned to highly dissolved atomic oxygen in silver. The bands at 650 and 950 cm^{-1} can be ascribed to the ν(Ag-O) vibrations for sub-surface species and ν(O-O) mode for adsorbed molecular oxygen.[43] Although, sub-surface species might promote adsorption of molecular oxygen, it could also be a probable consequence of surface restructuring in silver nanoparticles. Earlier reports mentioned two peaks centered at 630 and 800 cm^{-1}, as manifestations of sub-surface and strongly-bound atomic oxygen species respectively. The two bands are respectively predominant for Ag [110] and [111] planes.[43] The absence of the latter peak in our analysis supports the temperature induced restructuring of the crystal facets.

Conclusions

In conclusion, an environmentally friendly one-step synthesis of silver glyconanoparticles using sugar cane juice both as a reductant and a stabilizing agent has been reported. This method is general and can be applied to the synthesis of other

noble metal nanoparticles. Predominantly spherical or pseudospherical particles with increasing diameters (~5 nm to ~36 nm) are obtained with increase in salt concentration, temperature, solution pH and reaction time. The role of non-sugar moieties in addition to the sugar constituents of sugar-cane juice towards particle size and shape distribution and concomitantly material properties has been intimated. Furthermore, fluorescence and magnetic properties of the particles thus synthesized have also been quantified. A soft ferromagnetism was identified in the synthesized silver nanoparticles with approximate coercive filed value of 100 Oe. This green approach may be harnessed for a host of applications like studying cell/carbohydrate interactions, drug delivery, luminescent biological labels, magnetic resonance imaging and so on. Annealing of silver glyconanoparticles at 250 ^{o}C and 800 ^{o}C were studied. Annealing on an underlying layer of polymer fibers engendered fluorescent helical structures which might have potential applications in fabrication of nanocircuits. Rods generated on pristine silicon surface post-annealing might also be leveraged for opto-electronic applications.

Acknowledgements

The authors acknowledge the financial support provided by Department of Science and Technology and the DST Unit of Excellence on Soft Nanofabrication at IIT Kanpur.

Notes and references

[a] *Department of Chemical Engineering, Indian Institute of Technology, Kanpur, Kanpur-208016, India*
[b] *Present Address: Material Science and Engineering, University of Illinois, Urbana Champaign, 1304 W. Green St., Urbana, IL 61801, USA*
**Corresponding Author: Email: ashutos@iitk.ac.in; Tel: +91-512-2597026; Fax: +91-512-2590104*

Electronic Supplementary Information (ESI) available: Supplementary figures and tables. See DOI: 10.1039/b000000x/

1. P. R. Sajanlal, T. S. Sreeprasad, A. K. Samal and T. Pradeep, *Nano Reviews*, 2011, **2**, 5883-5944.
2. P. K. Jain, X. Huang, I. H. El-Sayed and M. A. El-Sayed, *Acc Chem Res* 2008, **41**, 1578-1586.
3. H. I. Peng, C. M. Strohsahl, K. E. Leach, T. D. Krauss and B. L. Miller, *ACS Nano*, 2009, **3**, 2265-2273.
4. K. A. Willets and R. P. V. Duyne, *Annu Rev Phys Chem*, 2007, **58**, 267-297.
5. R. R. Arvizo, S. Bhattacharyya, R. A. Kudgus, K. Giri, R. Bhattacharya and P. Mukherjee, *Chem Soc Rev*, 2012, **41**, 2943-2970.
6. C. M. Niemeyer, *Angew Chem Int Ed*, 2001, **40**, 4128-4158.
7. K. El-Boubbou, D. C. Zhu, C. Vasileiou, B. Borhan, D. Prosperi, W. Li and X. Huang, *J Am Chem Soc*, 2010, **132**, 4490-4499.
8. N. R. Jana, L. Gearheart and C. J. Murphy, *Chem Comm*, 2001, **0**, 617-618.
9. R. Jin, Y. Cao, C. A. Mirkin, K. L. Kelly, G. C. Schatz and J. G. Zheng, *Science*, 2001, **294**, 1901-1903.
10. Y. Sun and Y. Xia, *Science*, 2002, **298**, 2176-2179.
11. J. Zhang, S. Li, J. Wu, G. C. Schatz and C. A. Mirkin, *Angew. Chem. Int. Ed*, 2009, **48**, 7787-7791.
12. E. Katz and I. Willner, *Angew Chem Int Ed*, 2004, **43**, 6042-6108.
13. S. Singh, P. Patel, S. Jaiswal, A. A. Prabhune, C. V. Ramana and B. L. V. Prasad, *New J. Chem*, 2009, **33**, 646 - 652
14. J. M. d. l. Fuente and S. Penadés, *Biochim Biophys Acta*, 2006, **1760**, 636-651.
15. S. Singh, V. D'Britto, A. A. Prabhune, C. V. Ramana, A. Dhawan and B. L. V. Prasad, *New J. Chem.*, 2010, **34**, 294 - 301.
16. J. Zhang, C. D. Geddes and J. R. Lakowicz, *Anal Biochem*, 2004, **332**, 253-260.
17. H. Huang, Q. Yuan and X. Yang, *Colloids Surf. B: Biointerfaces*, 2004, **39**, 31-37.
18. S. Nazir, T. Hussain, M. Iqbal, K. Mazhar, A. G. Muazzam and M. Ismail, *J Biosci Technol*, 2011, **2**, 425-430.
19. M. C. Moulton, L. K. Braydich-Stolle, M. N. Nadagouda, S. Kunzelman, S. M. Hussain and R. S. Varma, *Nanoscale*, 2010, **2**, 763-770.
20. M. N. Nadagouda and R. S. Varma, *Green Chemistry*, 2008, **10**, 859-862.
21. Q. Zhou, B. Wang, P. Wang, C. Dellago, Y. Wnag and Y. Fang, *CrystEnggComm.*, 2013, **15**, 5114-5118.
22. D. Horton, ed., *Advances in carbohydrate chemistry*, Academic Press, San Diego, 1997.
23. S. He, J. Yao, P. Jiang, D. Shi, H. Zhang, S. Xie, S. Pang and H. Gao, *Langmuir*, 2001, **17**, 1571-1575.
24. M. I. Azócar, H. Muñoz, P. Levin, N. Dinamarca, G. Gómez, A. Ibañez, M. T. Garland and M. A. Paez, *Comm Inorg Synth*, 2013, **1**, 19-21.
25. A. Henglein and M. Giersig, *J. Phys. Chem. B*, 1999, **103**, 9533-9539.
26. S. Banerjee, K. Loza, W. Meyer-Zaika, O. Prymak and M. Epple, *Chem. Mater.*, 2014, **26**, 951-957.
27. D. Li, M. H. Nielsen, J. R. Lee, C. Frandsen, J. F. Banfield and J. J. D. Yoreo, *Science*, 2012, **336**, 1014-1018.
28. Y. Xiong, I. Washio, J. Chen, M. Sadilek and Y. Xia, *Angew Chem Int Ed*, 2007, **46**, 4917-4921.
29. M. R. Langille, M. L. Personick, J. Zhang and C. A. Mirkin, *J. Am. Chem. Soc.*, 2012, **134**, 14542-14544.
30. B. Tang, S. Xu, X. Hou, J. Li, L. Sun, W. Xu and X. Wang, *Appl Mater Sci Interfaces*, 2013, **5**, 646-653.
31. F.-T. Xie, H.-Y. Bie, L.-M. Duan, G.-H. Li, X. Zhang and J.-Q. Xu, *J. Solid StateChem.*, 2005, **178**, 2858-2866.
32. T. Zhang, G. Lu, H. Shen, K. Shi, Y. Jiang, D. Xu and Q. Gong, *Sci Reports*, 2014, **4**, 3867-3873.
33. Z. Jiang, W. Yuan and H. Pan, *Spectrochim Acta A*, 2005, **61**, 2488-2494.
34. X. Yang, L. F. Gan, L. Han, E. K. Wang and J. Wang, *Angew. Chem. Int. Ed.*, 2013, **52**, 2202-2206.
35. S. Fedrico, W. Harbich and J. Buttet, *J. Chem. Phys.*, 1993, **99**, 5711-5717.
36. K. N. K. Kowlgi, G. J. M. Koper, S. J. Picken, U.Lafont, L. Zhang and B. Norder, *Langmuir*, 2011, **27**, 7783-7787.
37. L. Suber, D. Fiorani, G. Scavia, P. Imperatori and W. R. Plunkett, *Chem Mater* 2007, **19**, 1509-1517.

38. M. Pereiro, D. Baldomir and J. E. Arias, *Phys Rev A*, 2007, **75**, 063204-063209.
39. H. Hori, Y. Yamamoto, T. Iwamoto, T. Miura, T. Teranishi and M. Miyake, *Phys Rev B* 2004, **69**, 174411-174415.
40. M. Hurtta, I. Pitkanen and J. Knuutinen, *Carbohydr. Res.*, 2004, **339**, 2267-2273.
41. A. Courty, A.-I. Henry, N. Goubet and M.-P. Pileni, *Nat. Mat.*, 2007, **6**, 900-907.
42. B. Radha and G. U. Kulkarni, *Cryst. Growth Des.*, 2011, **11**, 320-327.
43. G. J. Millar, M. L. Nelson and P. J. R. Uwins, *J. Chem. Soc., Faraday Trans.*, 1998, **94**, 2015-2023.

